Data supplement for Jaffe et al., Decoding Shared Versus Divergent Transcriptomic Signatures Across Cortico-Amygdala Circuitry in PTSD and Depressive Disorders. Am J Psychiatry (doi: 10.1176/appi.ajp.21020162)

Supplementary Results

Section 1. Cohort and sequencing data descriptions

The neurotypical control group was composed of 109 donors. The MDD group consisted of 109 patients with a diagnosis of MDD, but no comorbid PTSD diagnosis (DSM, 5th edition(1)). The PTSD group consisted of 107 patients with DSM-5 PTSD diagnosis. Types of trauma were characterized for all donors in the PTSD group - a majority were not exposed to combat (76.6%, **Table S2**), but rather had high rates of childhood maltreatment (66%, **Table S3**). Donors in the PTSD group also had high rates of comorbidity for MDD (62.6% with a comorbid diagnosis, **Table S2**), BD (27.1% with a comorbid diagnosis, **Table S2**) and substance use disorder (SUD) (77.6% with a comorbid diagnosis, **Table S2**).

We performed principal component analysis (PCA) of these data to better characterize global patterns of gene expression (**Figure S1C**). Top components of gene expression variation related to brain region and various measures of RNA quality (**Figures S1D**), with the first principal component (PC1, 20.4% of variance explained) associating strongly with RNA quality **(Figure S1E**), and distinguishing broad cortical and amygdala regions (with smaller differences within subregions, particularly within the amygdala (**Figure S1F**). While there were differences in some RNA-seq metrics, like the exonic mapping rate, by sample processing plate, these differences did not manifest in PC1. These data recapitulate established cytoarchitecture, as we observed greater local expression homogeneity among amygdala nuclei than cortical subregions, with greater amygdala similarity to the dACC than the dlPFC (2). We employed quality surrogate variable analysis (qSVA) (3), which defines degradation-susceptible genes across dlPFC and broad amygdala (see Methods), for downstream differential expression and network analyses to control for both observed and latent potential confounders.

Section 2. Expression differences related to PTSD diagnosis

Since subregions from the same broader regions showed more similar global expression patterns (**Figure S1F)**, we hypothesized that conducting primary analyses where subregions within the cortex and then the amygdala were combined to assess broader cortex and amygdala could increase statistical power to detect differentially expressed genes. We therefore identified the effects of PTSD versus neurotypical controls using linear mixed effects modeling within 641 broader cortex samples and then within 644 broader amygdala samples (including MDD samples, see Methods), allowing for differential PTSD versus neurotypical control effects within subregions (while simultaneously estimating MDD versus control effects, see Methods).

Sensitivity analyses for additional confounders involved adjusting our full DE model for each considered confounder sequentially, and examining if/how the PTSD effects attenuated. We calculated bias metrics of effect estimates (i.e. $$\beta$$ in the regression model, here the log2 fold change), as: |adjusted $$\beta$$ - original $$\beta$$ | / |original $$\beta$$| within each of the four brain regions for both PTSD and MDD among respective genes with $p < 0.05$. The median marginally significant gene only changed 9.6-13.2% across the various comparisons.

Similarly, 97% (all but three) of FDR < 0.1 DEGs for PTSD (ie those displayed in **Table 1**) showed at p < 0.005 significance in the sensitivity model for opiates.

We performed more in-depth analyses around childhood maltreatment and combat exposures. We performed differential expression analyses within each brain region, first comparing donors with (N=94) versus without (N=223) childhood maltreatment (controlling for the same technical and clinical variables, except ignoring primary groups of PTSD, MDD and Control) - 8 donors in the Control group were missing information on childhood maltreatment, and were thus excluded. When combining diagnostic groups, and assessing the transcriptional effects of childhood maltreatment, we only found DEGs in MeA (4 genes at FDR < 0.1 and 7 genes at FDR < 0.2; ranked: *KIAA1551*, *FTCDNL1*, *DUSP4*, *HES1*, *AC012370.2*, *SQRDL*, and *PPP1R3C*). However, we found higher global correlation between t-statistics for childhood maltreatment compared to PTSD than MDD, in line with the increased prevalence of this exposure among the PTSD (66%) compared to MDD (20%) groups. We performed analogous analyses using combat exposure, comparing 28 combat-exposed donors to 289 unexposed donors. We found two genes significantly differentially expressed in at least one brain region at FDR < 0.05 (*GSTM1*: dACC, dlPFC, MeA; *LINC01411*: MeA) and a third relaxing to FDR < 0.2 (*CSF3*: BLA).

We attempted to confirm our PTSD DEGs using results from a recent manuscript that used a subset of the same donors used in this study (N=56) in the dACC (4). Across the 57 genes considered expressed in those data (of 72 identified here), 46 were directionally consistent (80.7%), and 9 were further genome-wide significant (15.8%, at FDR< 0.1), with highly correlated log2 fold changes across these 57 genes (ρ=0.58, p=1.56e-6, **Figure S7A**). Analogous analyses using the 193 expressed DEGs in those data (among 196 identified) showed similar directional consistency (82.3%) and correlation (ρ=0.56) of $\log_2$ fold changes in our data, but had a much lower overall confirmation replication rate (9/193, 4.7%). Another key difference between studies involved the inclusion of patients with BD in this study's PTSD group. Sensitivity analyses in the dACC excluding the 28 donors in the PTSD group with a comorbid BD diagnosis yielded highly concordant DEGs as identified in the full dataset (via global t-statistic correlation, \rho = 0.963). Additional analyses comparing the PTSD (n=77) versus BD (n=28) primary diagnoses within the PTSD group showed little global correlation to the full PTSD versus control group effects (\rho = 0.11), and identified a single significant gene (*RPL13P12,* p=5.4e-8), which was not a PTSD (versus control) DEG (p=0.41).

Section 3. Gene sets and cell types associated with PTSD

We used cell type-specific reference profiles generated with translating ribosomal affinity purification (TRAP) techniques from transgenic BACarray reporter mice (5–7) for these enrichment analyses because molecular annotations from the human brain are largely restricted to data obtained from single nucleus RNA sequencing (snRNA-seq), which lacks expression data from neuronal processes (8).

We note that the reference cell type profile for Layer 5a corticostriatal interneurons (Ctx.etv1_ts88) was indicated as containing contamination with lymphoid cells (immune cells including microglia) (5,6). These findings were robust to the choice of cellular specificity of input genes (specificity threshold/pSI ranges from 0.05 to 1e-4, **Table S5**) and convergent with the gene set enrichment analyses described above, particularly related to decreased expression of immune-related gene sets in PTSD.

Section 4. WGCNA analyses

WGCNA was at the broad region and then subregion levels, analogous to differential expression analyses models above. This approach assigns each gene to an individual module ("module membership") and then computes an "eigengene" for each sample and each module (corresponding to the first principal component of all genes in that module). We first tested for enrichment of module membership among marginally differentially expressed genes (at p <0.005) identified for PTSD versus neurotypicals and MDD versus neurotypicals. There were 35 total modules enriched for genes implicated in either disorder (at FDR < 0.05, odds ratio, OR>1; PTSD: 22 modules, MDD: 22 modules, with 9 in common). We further tested for module eigengene associations with PTSD, MDD, and PTSD-specific diagnoses for convergent evidence implicating each module with each disorder, and annotated each module with the most significant gene ontology-enriched category

We performed a series of sensitivity analyses, specifically further including each of: combat, childhood maltreatment, and then toxicology-determined smoking, SSRI antidepressant use, and opioid use in the ME ~ Dx modeling [e.g. evaluating "combat" involved modeling ME ~ Dx + Combat]. Only 4 modules showed any association (at $p < 0.01$) to these other covariates: Cortex_ME31 (combat p=0.0055), dlPFC_ME3 (combat p = 0.0064), Amygdala_ME2 (childhood maltreatment p = 0.0061), Amygdala_ME19 (opioid use p=0.004). Interestingly, PTSD was associated with: Cortex_ME31 and become more significant when adjusting for combat (p=0.032 to p=0.0077) and Amygdala_ME2 became more significant when adjusting for childhood maltreatment (p=0.0047 to p=0.00053). Similarly, MDD was associated with dlPFC_ME3, with unchanged effects further adjustment of combat (p=0.002 to 0.002) and with Amygdala_ME19, which became less significant when adjusting for opioid use (p=0.005 to 0.32).

Supplementary Methods

Human brain tissue

Postmortem human brains were donated through US medical examiners' offices at the time of autopsy (total N=326), including the Office of the Chief Medical Examiner of: the State of Maryland (n=279), the District of Columbia (n=6), and of Virginia, Northern District (n=16), Western Michigan University Homer Stryker MD School of Medicine, Department of Pathology (n=24), and University of North Dakota Forensic Pathology Practice Center, Grand Forks County Coroner's Office (n=1). Legal next-of-kin gave informed consent to brain donation according to protocols Maryland Department of Health and Mental Hygiene (MDHMH) # 12-24 (MD), National Institute of Mental Health (NIMH)# 90-M-014 (District of Columbia and Virginia), and Western Institutional Review Board (WIRB) # 1126332 (Maryland, Western Michigan University, University of North Dakota), respectively. Every brain received both a macroscopic and microscopic neuropathological examination at the time of autopsy by a board-certified neuropathologist. Brains were excluded from this study if there was evidence of cerebrovascular accidents, neuritic pathology, or other significant trauma to the brain that precluded it from further study.

The research conducted in this study was not considered human subjects research as defined by the HHS, as according to 45 CFR 46.102(f), a human subject is defined as a living individual about whom an investigator conducting research obtains data through intervention or interaction

with the individual or identifiable private information. This research involved the analysis of RNA from postmortem human tissue.

A retrospective clinical diagnostic review was conducted on every brain donor, consisting of the telephone screening, macroscopic and microscopic neuropathological examinations, autopsy and forensic investigative data, two sources of toxicology data, extensive psychiatric treatment, substance abuse treatment, and medical record reviews, and whenever possible, family informant interviews (i.e., next-of-kin could be recontacted and was agreeable to phone contact,, which included the PTSD Checklist (i.e., PCL-5 and/or the MINI). A history of traumatic exposure including exposure to military combat, physical abuse, sexual abuse, emotional abuse, and/or other traumas were obtained as part of the telephone screening, records reviews, and/or PCL-5. A board-certified psychiatrist with expertise in PTSD reviewed every case in this study to rate presence/absence of PTSD symptoms. A summary of the trauma information is in Table S3.

All data were compiled into a comprehensive psychiatric narrative summary that was reviewed by two board-certified psychiatrists in order to arrive at lifetime DSM-5 psychiatric diagnoses (including substance use disorders/intoxication) and medical diagnoses. Non-psychiatric healthy controls were free from psychiatric and substance use diagnoses, and their toxicological data was negative for drugs of abuse. Every brain donor had either a medical examiner toxicological analysis, which typically covered ethanol and volatiles, opiates, cocaine and metabolites, amphetamines, and benzodiazepines. Every donor also received supplemental directed toxicological analysis using National Medical Services, Inc., including nicotine/cotinine testing, cannabis testing, and the expanded forensic panel in postmortem blood (or, in rare cases, in postmortem cerebellar tissue) in order to cover any substances not tested. The presence of opioids was determined by toxicology evaluations, including: codeine, morphine, oxycodone, hydrocodone, oxymorphone, hydromorphone, methadone, propoxyphene, fentanyl, 6-acetylmorphine (an active metabolite of heroin), and tramadol. If the medical examiner specifically noted the presence of any other opioids, then the subject was also included in this count.

Tissue dissections

dACC (BA24/32): The dorsal anterior cingulate gyrus was identified visually on 1 cm thick coronal slab, on the mesial surface of the frontal lobe at the level of the genu of the corpus callosum. Gray matter from the cortical ribbon of the dACC, which was identified as the gyrus immediately dorsal to the corpus callosum, was dissected from the slab using a hand-held dental drill while the slab was positioned on dry ice after being removed from storage in a –80 C freezer.

dlPFC (BA9/46): Under direct visual guidance using a hand held dental drill, for the dorsolateral prefrontal cortex (dlPFC) dissections, grey matter tissue from the cortical ribbon was dissected from the crown of the middle frontal gyrus, from the coronal slab immediately anterior to the genu of the corpus callosum. Subcortical white matter was carefully trimmed from the area immediately below the middle frontal gyrus.

Amygdala: The medial and baso-lateral amygdaloid nuclei were dissected from the mesial superior temporal lobe for 0.75-1 cm thick coronal slabs of frozen human brains on dry ice using a stainless steel punch (8mm diameter Thermo Fisher Scientific Integra Miltex standard biopsy punch). Amygdaloid nuclei were dissected at the level of the anterior commissure, anterior thalamus and lentiform nucleus, which corresponded to the middle part of the amygdala along

its anterior to posterior axis (9,10). Tissue punch weights were in the range of 100-150 mg and were further powdered in frozen state before downstream extractions to ensure minimal sampling variability across all subjects in the study.

RNA sequencing

Total RNA was extracted from all 1304 tissue samples using AllPrep DNA/RNA Mini Kit (Qiagen Cat No./ID: 80204) to concurrently extract RNA and DNA from the same piece of homogenized tissue in brain region- and diagnostic group-balanced batches of 96 samples. Paired-end strand-specific sequencing libraries were prepared from 300ng total RNA using the TruSeq Stranded Total RNA Library Preparation kit with Ribo-Zero Gold ribosomal RNA depletion which removes rRNA and mtRNA . An equivalent amount of synthetic External RNA Controls Consortium (ERCC) RNA Mix 1 (Thermo Fisher Scientific) was spiked into each sample for quality control purposes. RNA-seq cDNA libraries were genotyped with qPCR across 33 SNPs to establish sample identities with a genotype barcode. The libraries were then sequenced on an Illumina HiSeq 3000 at the LIBD Sequencing Facility, producing a median of 131.3 million (IQR: 115.4-146.3) fragments (across 100-bp paired-end reads) per sample.

RNA-seq processing pipeline

Raw sequencing reads were processed using the same pipeline described in detail in Collado-Torres et al (11). Briefly, paired-end reads were mapped to the hg38/ GRCh38 human reference genome with splice-aware aligner HISAT2 version 2.0.4 (12). Feature-level quantification based on GENCODE release 25 (GRCh38.p7) annotation was run on aligned reads using featureCounts (subread version 1.5.0-p3) (13) with a median 43.8% (IQR: 37.3%-49.0%) of mapped reads assigned to genes. Exon-exon junction counts were extracted from the BAM files using regtools v.0.1.0 (14) and the bed_to_juncs program from TopHat2 (15) to retain the number of supporting reads (in addition to returning the coordinates of the spliced sequence, rather than the maximum fragment range) as described in Jaffe et al. (16). Annotated transcripts were quantified with Salmon version 0.7.2 (17) and the synthetic ERCC transcripts were quantified with Kallisto version 0.43.0 (18). For an additional QC check of sample labeling, variant calling on 740 common missense SNVs (containing the above 33 cDNA-genotyped SNPs) was performed on each sample using bcftools version 1.2. We generated strand-specific base-pair coverage BigWig files for each sample using bam2wig.py version 2.6.4 from RSeQC (19) and wigToBigWig version 4 from UCSC tools (20) for quality surrogate variable analysis (3) (as described below).

Genotype data processing

Genotype data were processed and imputed as previously described (16). Briefly, genotype imputation was performed on high-quality observed genotypes (removing low quality and rare variants) using the prephasing/imputation stepwise approach implemented in IMPUTE2 (21) and Shape-IT (22), with the imputation reference set from the full 1000 Human Genomes Project Phase 3 dataset (23), separately by Illumina platform using genome build hg19. There were a total of 5 imputed batches in the current study, with 4 of 5 batches using an Illumina Infinium Omni2.5-8 kit (versions 1.2 or 1.3), and the remaining batch of 37 samples using the Infinium Omni5-4 kit. Imputed genotypes were merged across imputation runs/batches in the Oxford file format as dosages, then converted to plink file format as "hard call" genotypes (treating variants with posterior probabilities < 0.9 as missing). We retained common variants (MAF > 5%) that were present in the majority of samples (missingness < 10%) and that were in Hardy Weinberg equilibrium (at $p > 1x10^{-6}$) using the Plink tool kit version 1.90b3a (24).

Multidimensional scaling (MDS) was performed on autosomal LD-independent SNPs (variation inflation factor = 1.25, corresponding to $R^2 < 0.2$) to construct genomic ancestry components on each sample, which can be interpreted as quantitative levels of ethnicity – the first component separated the Caucasian and African American samples, for inclusion as potential confounders in the differential expression analyses described below. The same 740 observed and imputed DNA-genotyped SNPs (as described above in the RNA-seq data processing) were further extracted across the 326 unique donors.

Quality control and sample filtering

After completing the preprocessing pipeline on 1304 RNA-seq samples across 326 donors, we performed quality control assessments, including for sample identities and RNA-seq data quality. We first computed the pairwise genotype correlations across the 1304 RNA-seq samples among 235/740 high quality and moderate coverage variants (mean depth between 5-80, biallelic variants, and variant distance bias - VDB - p-values greater than 0.1). From this 1304 RNA x 1304 RNA correlation matrix, we expected clusters of four samples per donor, with high correlations among the 4 samples from the same donor and low correlations to all other samples. We subsequently computed the correlation between the 231/235 high-quality variants also present in the DNA-derived genotype data across these 326 donors (forming a 1304 RNA x 326 DNA correlation matrix). Here we expected each RNA sample to match DNA from its labeled donor. These two correlation matrices allowed us to a) identify and b) potentially recover sample identities, and comparison to the 33 cDNA genotypes further refined the processing steps where sample swaps occurred. Overall, 19 RNA-seq samples were dropped due to sample mis-identity issues, including 5 samples with sample contamination (two genomes in the RNA-seq library) and 11 samples with genotyping issues inconsistent with the study design (i.e. a fifth sample from the same donor with one region repeated) and 3 samples first identified in the cDNA libraries and confirmed in the RNA-seq libraries. The 5 samples with contaminations were identified by moderate correlations to DNA genotypes (~0.4-0.6) and were indicative of pipetting issues during library preparations resulting in library mixing, as examinations of these mixed samples were always in adjacent wells on the 96 well preparation plates. There were 8 additional samples (from 4 pairs) that were identified as pairwise sample swaps that were reversed, and one sample with a mislabeled brain number. Our final sample characterizations and analyses were therefore performed on 1285 RNA-seq samples.

We then examined the distribution of sequencing and RNA quality metrics across group-region pairs, flow cells, and processing plates (**Figure S1**, **Figure S12**). ERCC spike-ins were uniformly distributed across brain regions and diagnosis groups (all $p > 0.01$), while metrics related to RNA quality (exonic mapping rate, mitochondrial mapping rate, RNA integrity number, and genome alignment rate) varied by brain region (all ANOVA $p < 1e\text{-}4$) but not diagnosis (all ANOVA $p > 0.01$). Examination of analogous effects by processing plate showed differences in ERCC spike-ins between the first 6 compared to the next 8 plates (**Figure S12A**) and lower RNA quality for plates 3 and 13 (**Figure S12B**). As plates were balanced by the primary outcomes of interest (region and diagnosis), we retained these samples in all downstream analyses and subsequently adjusted for these variables in differential expression analyses to reduce variation attributable to technical factors.

Feature filtering by expression levels

We filtered lowly expressed features across all 1285 samples prior to expression analyses within and across brain regions. We calculated reads per kilobase per million (RPKM) genes (or exons) assigned during counting for genes and exons, and retained count data from 26,020

genes and 415,709 exons with RPKM > 0.2. Here we explicitly used the total number of gene or exon counts, and explicitly not the total number of aligned reads (which is sometimes used in RPKM calculations). We normalized exon-exon splice junction reads by scaling counts to 10 million reads with splice junctions (RP10M, analogous to total assigned gene counts for RPKM calculations). We used 10 million instead of 1 million both because it leads to easier visualization and because 10 million reads was the approximate number of spliced reads in an average library; this retained 217851 splice junction counts with RP10M > 0.75 that were at least partially annotated to one exon (ie annotated, exonic skipping or shifted exonic boundary junction classes). We lastly filtered pseudo-aligned normalized transcript counts (TPMs) using a cutoff of 0.2, leaving 101,515 transcripts for analysis.

Degradation data processing for qSVA

We calculated quality surrogate variables to account for potentially latent RNA quality confounding (3). Here we used already-available RNA-seq degradation profiles from dlPFC [neuron 2019] (20 samples: 5 brains and 4 time points) and bulk amygdala [zandi preprint] (20 samples: 5 brains and 4 time points), and implemented a combined-region approach akin to Collado-Torres et al 2019. We therefore calculated mean coverage separately by strand across all 40 combined samples to define expressed regions with greater than 5 normalized reads and greater than 50bp (25). We then fit a linear model to each expressed region as a function of degradation time adjusting for brain region and donor as fixed effects. We then ranked the expressed regions by the degradation effect and created an input bed file with the top 1000 degradation-susceptible regions for coverage-based quantification in the 1285 post-QC RNA-seq samples described above. Subsequently quality surrogate variables (qSVS) for each sample were calculated once for the entire project from the top k principal components (PCs) of the expression in these 1000 degradation regions across all 1285 samples. We selected k = 19 using the BE algorithm (26) with the sva Bioconductor package (27).

Differential expression analyses

We performed differential expression analyses across several different subsets of samples, for several different statistical models, at four feature summarizations. Our main analyses involved dividing this dataset into to regional groups: combining the two cortical regions (dlPFC + dACC) into a "cortex" dataset (N=641) and the two amygdala subregions (BLA + MedAmy) in an "amygdala" dataset (N=644). These analyses involved three groups of samples: neurotypical controls ("CONT", patients with major depression ("MDD") and patients with PTSD ("PTSD"), where the CONT group was generally the reference group in downstream regression analyses. Within each of these datasets, we fit one main statistical model that involved jointly estimating the effects of (a) PTSD vs CONT, (b) MDD vs CONT, (c) PTSD vs MDD, and (d) PTSD vs MDD vs CONT of the form:

$$y_{ij}\ \alpha_{ij} + \sum_{k=1}^{2} \beta_{ik} Dx_{ijk} + \zeta_i Region_j + \sum_{k} \gamma_{ik} Dx_{ijk} * Region_j + \omega_{Zj} + \delta_i qSVs_j + \varepsilon_{ij}$$

Where y_{ij} are voom-normalized feature counts (on the log2 scale) (28) for feature i and sample j, β_{i1} is the $\log_2$ fold change for PTSD vs Control and β_{i2} is the log_2 fold change for MDD vs Control. We adjusted for subregions in the cortex (ie dACC vs dlPFC) and amygdala (ie BLA vs MedAmy) analyses, as well as the statistical interaction between the subregion term and each diagnosis main effect term. We further adjusted for the vector of fixed effects potential observed

confounders "Z", including age, sex, chrM mapping rate, rRNA rate, exonic mapping rate, RIN, overall mapping rate, the ERCC bias factor (e.g. root mean square error) and then quantitative ancestry factors 1,2,3, 8, 9, and 10 (which were all associated with diagnosis groups). We further adjusted for the vector of fixed effects latent confounders "qSVs" (specifically 19 qSVs, described above). Here, as there were multiple regions from the same donors, α_{ij} was parameterized as a random intercept using the `duplicateCorrelation` function in limma, with donor as the blocking variable. We therefore used linear mixed effects modeling (rather than regular linear regression) to fit the above model, once to the "cortex" dataset, and again to the "amygdala" dataset. PTSD vs CONT, MDD vs CONT, and PTSD vs MDD effects were converted to empirical Bayes-moderated T-statistics, with corresponding p-values, and Benjamani-Hochberg-adjusted (BH-adjusted) p-values using the limma topTable function. We also used the topTable function to calculate an F-statistic to test mean differences between the three diagnosis groups from β_{ik}, with corresponding p-values and BH-adjusted p-values. We fit secondary models to the "cortex" and "amygdala" datasets recoding the diagnosis group variable into a binary "PTSD-only" variable, comparing patients with PTSD (coded as 1) to a combined MDD and Control group (coded as 0) to estimate PTSD-specific effects with the exact same adjustment terms as the standard three-level diagnosis variable. We further fit secondary models to the "Joint"/combined dataset of all 1285 samples with linear mixed effects modeling, where there were 3 region terms (instead of 1 above) and 6 region-by-diagnosis interaction terms (instead of 2 above) which were used to calculate overall diagnosis effects across all regions as well as an F-statistic per model for overall diagnosis-by-region interaction effects. We lastly fit secondary models within each subregion using linear regression (since there were no repeated donors within each region) and dropped main effect and interaction terms related to region from the above model (ie $$\zeta$$ and $$\gamma$$) to estimate the effects of diagnosis within each region. We fit these models separately at the feature levels of genes, exons, junctions, and transcripts. As we used TPMs rather than raw counts for transcript-level analyses, we skipped the voom step.

Gene Ontology and gene set enrichment analyses

Unless otherwise noted, we used the compareCluster() function from clusterProfiler (29) version 3.14.3 for gene ontology (30,31) and KEGG (32) enrichment analyses with the set of Ensembl gene IDs expressed in genes.

RNA deconvolution

We used a previously-published reference/signature matrix for 10 neural cell types, and an analogous RNA deconvolution strategy, in Burke, Chenoweth et al. (33). The signature matrix is available at: https://raw.githubusercontent.com/LieberInstitute/libd_stem_timecourse/master/deconvolution/cell_type/singleCell_iPSC_quake_coefEsts_calibration_Zscale.csv . We deconvolved RNA fractions of the 10 cell types, and tested for differences across diagnosis groups and brain regions. We also performed correlation between each RNA fraction and each qSV.

WGCNA

We performed weighted gene co-expression network analysis (WGCNA) using the WGCNA R package (34) (package version 1.69 and R version 3.6.1). WGCNA analyses were performed in the four brain regions separately as well as in the two broad region groups (amygdala and

cortex) and the full dataset, resulting in 7 total WGCNA analyses. After filtering out lowly expressed genes (cutoff mean RPKM > 0.2), the $\log_2$(RPKM+1) normalized expression values were "cleaned" using the cleaningY function from the jaffelab R package (35) (version 0.99.30). Specifically, the same covariates as modeled above were regressed out of the expression matrix: mitochondrial RNA rate; rRNA rate; gene assignment rate; RIN; mapping rate; ERCC spike-in error; genomic ancestry components 1, 2, 3, 8, 9, and 10; and latent quality surrogate variables 1-19, while preserving the effects of diagnosis, age and sex, and, when applicable, brain region and their interaction (in the combined-region analyses). WGCNA was run using the same strategy for each of the seven runs: automated determination of the soft thresholding parameter (using the `pickSoftThreshold` function), and then constructing co-expressed modules (using the `blockwiseModules` function) using signed networks with "bicor" correlation, with a minimum module size of 30, mergeCutHeights of 0.25, and no reassignment. We applied gene ontology enrichment analysis (GO) using clusterProfiler (29) (version 3.14.3) to understand the biological enrichments of our clusters. We subsequently tested the association between each module eigengene and diagnosis, adjusting for age, sex for single-region analyses, and further adjusted for brain region, and the interaction between brain region and diagnosis, as well as random effects of donors, when performing multi-region analyses. Note we did not account for the other confounders as their effects were regressed out of the expression data prior to module construction.

Sensitivity analyses

For each of the four brain regions, we performed sensitivity analyses for the following observed covariates sequentially: opioid use (based on toxicology), exposure to trauma (lifetime, based on narratives/medical history), antidepressant use (based on toxicology), antidepressant use (lifetime, based on narratives/medical history), and manner of death (natural, suicide, undetermined, accidental). For each sensitivity analysis - which considered a single confounder from the previous list, we adjusted the original model (above) to include each additional covariate, and then compared the original regression coefficients for each diagnosis (β) to the further-adjusted diagnosis coefficient (β^c, such that we ran 5 different sensitivity analyses)

$$y_{ij} = \alpha_i + \beta_i^c Dx_j + \gamma_i Covs_j + \zeta_i qSV_j + \delta_i Var_j + \varepsilon_{ij}$$

Childhood maltreatment and combat exposure differential expression analyses

We first performed differential expression analyses within each brain region comparing donors with (N=94) versus without (N=223) childhood maltreatment (controlling for the same technical and clinical variables, except ignoring primary groups of PTSD, MDD and Control, using the same methods as above). There were 8 donors in the Control group who were missing information on childhood maltreatment, and were thus excluded. We performed analogous analyses comparing 28 combat-exposed donors to 289 unexposed donors within each brain region across all donors. We lastly performed analogous analyses within just the PTSD group, comparing the 25 combat-exposed donors with PTSD to the 82 PTSD donors without combat exposure within each brain region.

Cell type enrichment analyses

We used functionality in the CSEA package to estimate cell type enrichments using pre-defined gene sets obtained from Mouse BAC-trap lines (7). We performed an analogous form of CSEA for human cell types using Fisher's exact tests on pre-defined cell type-specific genes described in Tran et al (36), Velmeshev et al (37) and Mathys et al (38) .

RNAscope single molecule fluorescence *in situ* hybridization

Postmortem dlPFC and BLA were dissected as previously described from two adult males with no known psychiatric illnesses. Brain tissue was equilibrated to −20°C in a cryostat (Leica, Wetzlar, Germany) and serial sections of dlPFC and BLA were collected at 10 µm. Sections were stored at −80°C until completion of the RNAscope assay.

We performed *in situ* hybridization with RNAscope technology utilizing the RNAscope Fluorescent Multiplex Kit V2 (Cat # 323120 Advanced Cell Diagnostics [ACD], Hayward, California) according to manufacturer's instructions and as previously described (39). Briefly, tissue sections were fixed with a 10% neutral buffered formalin solution for 30 min at room temperature, series dehydrated in ethanol, and pretreated with hydrogen peroxide at RT for 10 minutes then with protease IV for 30 min. Sections were incubated with a custom-designed Channel 4 *CORT* probe (Cat # 593341-C4, Advanced Cell Diagnostics, Hayward, California) and commercially available *CRHBP*, *GAD2*, and *SST* probes (Cat #s 573411, 415691-C3, 310591-C2) for 2 hours and stored overnight in 4x SSC (saline-sodium citrate) buffer. Probes were fluorescently labeled with Opal dyes (PerkinElmer, Waltham, MA). Opal dyes were diluted at 1:500 and assigned to each probe as follows: Opal520 to *CRHBP*, Opal570 to *SST*, Opal620 to *CORT,* and Opal690 to *GAD2*). Confocal lambda stacks were acquired using a Zeiss LSM 780 equipped with a 63X/1.4NA objective, a GaAsP spectral detector and 405, 488, 561, and 647 lasers. All lambda stacks were acquired using the same laser intensities, linear unmixing performed as previously described, and images were processed with our dotdotdot software (39). Summarized nuclei/ROI-level and transcript/dot-level data were analyzed using Pearson correlation analyses in R.

Given the low prevalence of *CORT* and *SST* transcripts, we captured images from locations in tissue sections of the BLA where *CORT* and/or *SST* were expressed **Figure 3A**) for a total of 489 nuclei/regions-of-interest (ROIs) across 32 images (see Methods). Almost all *SST*+ interneurons co-expressed *CORT* (64/65 ROIs using 5 dot cutoff to classify as "expressed") whereas only 64/183 *CORT*+ interneurons co-expressed *SST*. Our top amygdala DEG - *CRHBP* - showed co-expression with *CORT* and *GAD2* across many ROIs in both brain regions (40,41).

Supplementary Table Legends

The supplementary tables are provided in an accompanying Excel file.

Table S1: RNA integrity number (RIN) differences across brain subregions and diagnosis groups. PTSD vs Control and PTSD vs MDD p-values are based on linear regression and ANOVA P-value is based on differences in means across 3 groups using F test.

Table S2: PTSD group demographics and comorbidities against combat exposure. P-value is based on Chi-squared test.

Table S3: Detailed descriptions of trauma types. Reporting the percentage of donors in each group in each trauma category. Donors can have more than one type of trauma.

Table S4: Mean RNA sequencing and quality metrics across brain regions and diagnosis groups. The last three columns report ANOVA F-test p-values based on a linear model of: Measure ~ Region + Subregion + Group.

Table S5: Assessing the differences in PTSD effects within versus across sexes. T-statistics for the PTSD effect in each brain region are reported for each gene (ie dACC column), and then the differences in PTSD t-statistics in females versus PTSD t-statistics in males are reported (ie dACC_FvM column). Genes with large absolute FvM values have larger differences in PTSD effects in males and females.

Table S6: Differential expression statistics for combat exposure in PTSD group within each brain region. logFC = log2 fold change; t = moderated t-statistic/ Z-score; adj.P.Val = Benjamini-Hochberg adjusted p-value, controlling the false discovery rate.

Table S7: Gene Ontology enrichment statistics for PTSD (versus control) DEGs identified in each brain region or subregion. All DEGs are considered together ("Both") or stratified by directionality ("Up", higher expression in PTSD versus controls and "Down", lower expression in PTSD versus controls). Count = number of DEGs in gene set, p.adjust = Benjamini-Hochberg adjusted p-value, controlling the false discovery rate

Table S8: CSEA statistics for PTSD (versus control) DEGs identified in each brain region or subregion. Comparison = which PTSD DEG set is being utilized (see Table S7 legend), psi = set specificity index, with lower psi corresponding to more set-specific genes.

Table S9: Reporting -log10 p-values for human cell type enrichment analyses of PTSD (versus control) DEGs using snRNA-seq reference datasets. Positive values reflect being enriched and negative values reflect being depleted. First set of statistics relates to amygdala and the next several sets relate to cortex.

Table S10: Gene Ontology enrichment statistics for MDD (versus control) DEGs identified in each brain region or subregion. See legend for Table S7 for description of columns.

Table S11: CSEA statistics for MDD (versus control) DEGs identified in each brain region or subregion. See legend for Table S8 for description of columns.

Table S12: Gene Ontology enrichment statistics for PTSD versus MDD DEGs identified in each brain region or subregion. See legend for Table S7 for description of columns.

Table S13: CSEA statistics for PTSD versus MDD DEGs identified in each brain region or subregion. See legend for Table S8 for description of columns.

Table S14: WGCNA module membership of genes. Cells of the table correspond to which module each gene was assigned in each separate WGCNA run (0 = grey module, unassigned)

Table S15: Complete WGCNA enrichment statistics (analogous to Table 3), including enrichments of gene membership to GO and human snRNA-seq data. Columns with _t or _p represent eigengene associations to group and columns with _OR or _Pval represent enrichment statistics of DEGs to module membership. GOBP = Gene Ontology biological process, GOMF = Gene Ontology molecular function, GOCC = Gene Ontology cellular compartment.

Supplementary Figures

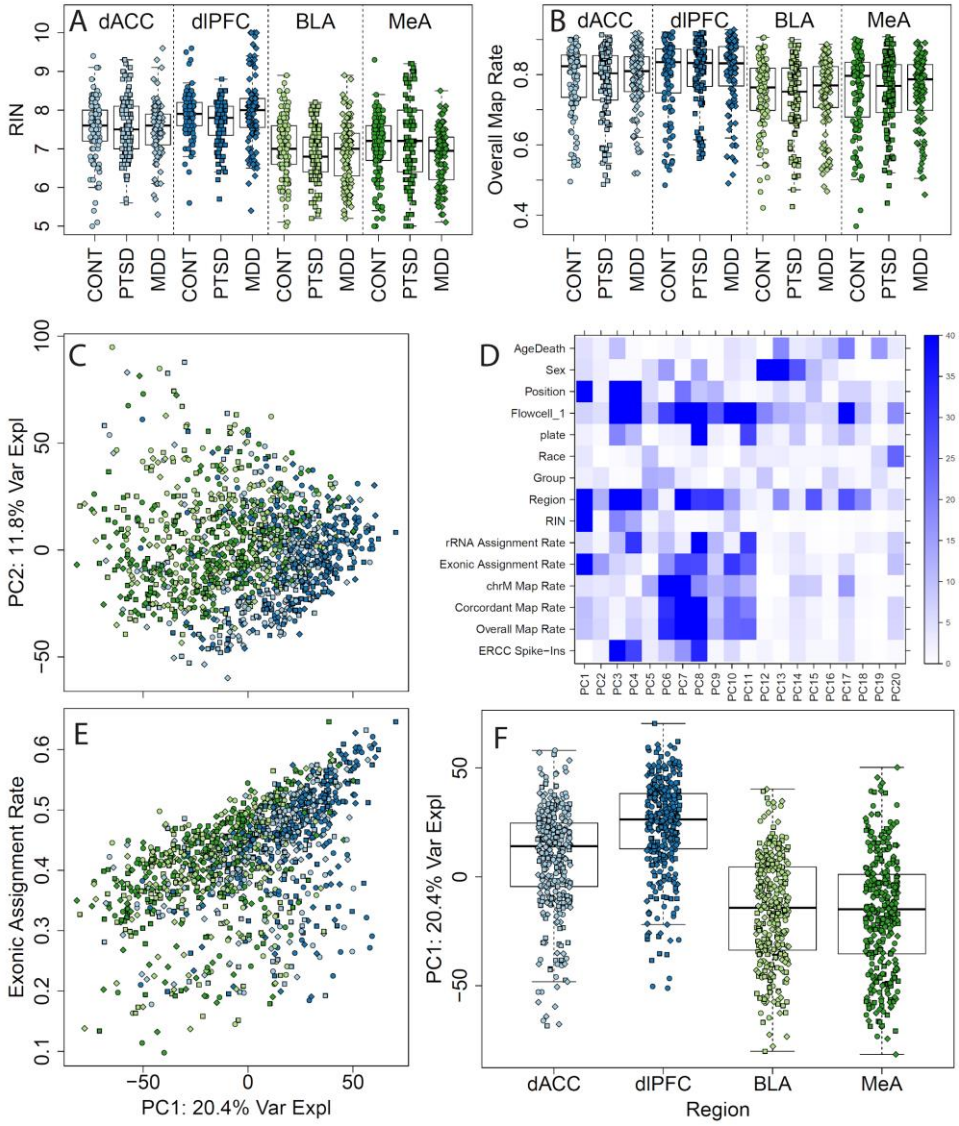

FIGURE S1. RNA quality and sequencing metrics. (A) RNA integrity numbers (RINs) and (B) overall RNA-seq read mapping rates across brain regions and diagnosis groups. (C) Principal component (PC) 1 versus 2 shows differences by brain region. (D) Associating observed clinical and technical variables with gene expression PCs, colors are negative log10 p-values from linear regression (either single terms for continuous or binary variables and ANOVA group p-values for categorical variables). (E) Exonic assignment rate (i.e. the fraction of aligned reads that were assigned to genes during counting) and (F) brain region, particularly cortex versus amygdala, associates with PC1 as well.

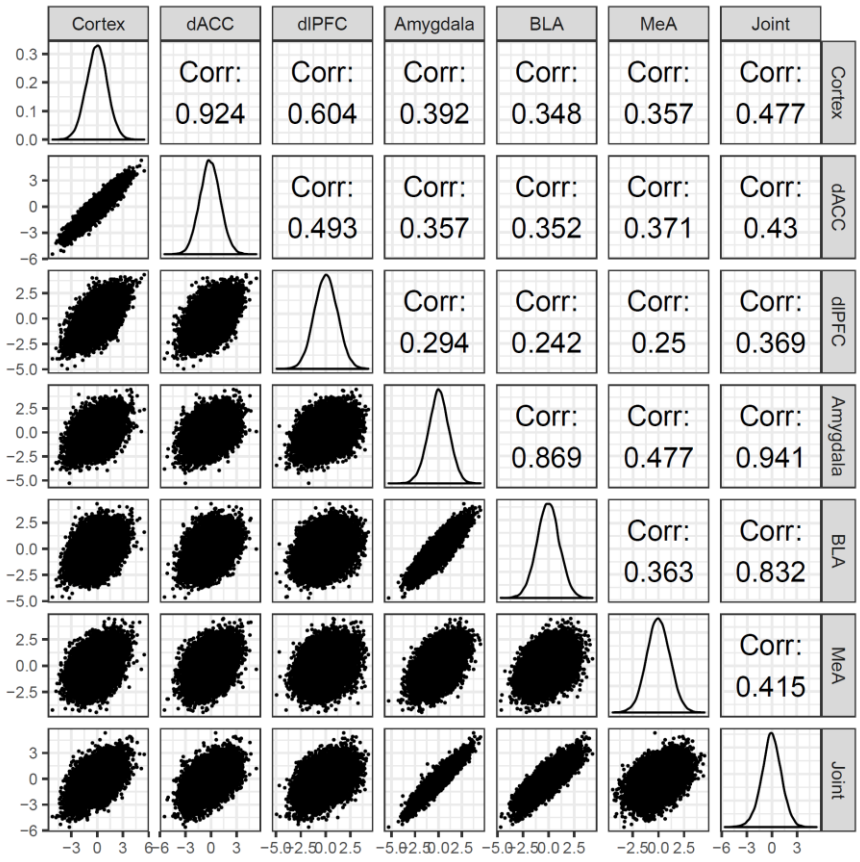

FIGURE S2. High gene-level correlations between PTSD effects (as Z-scores) across different subsets of samples, both within and across brain subregions.

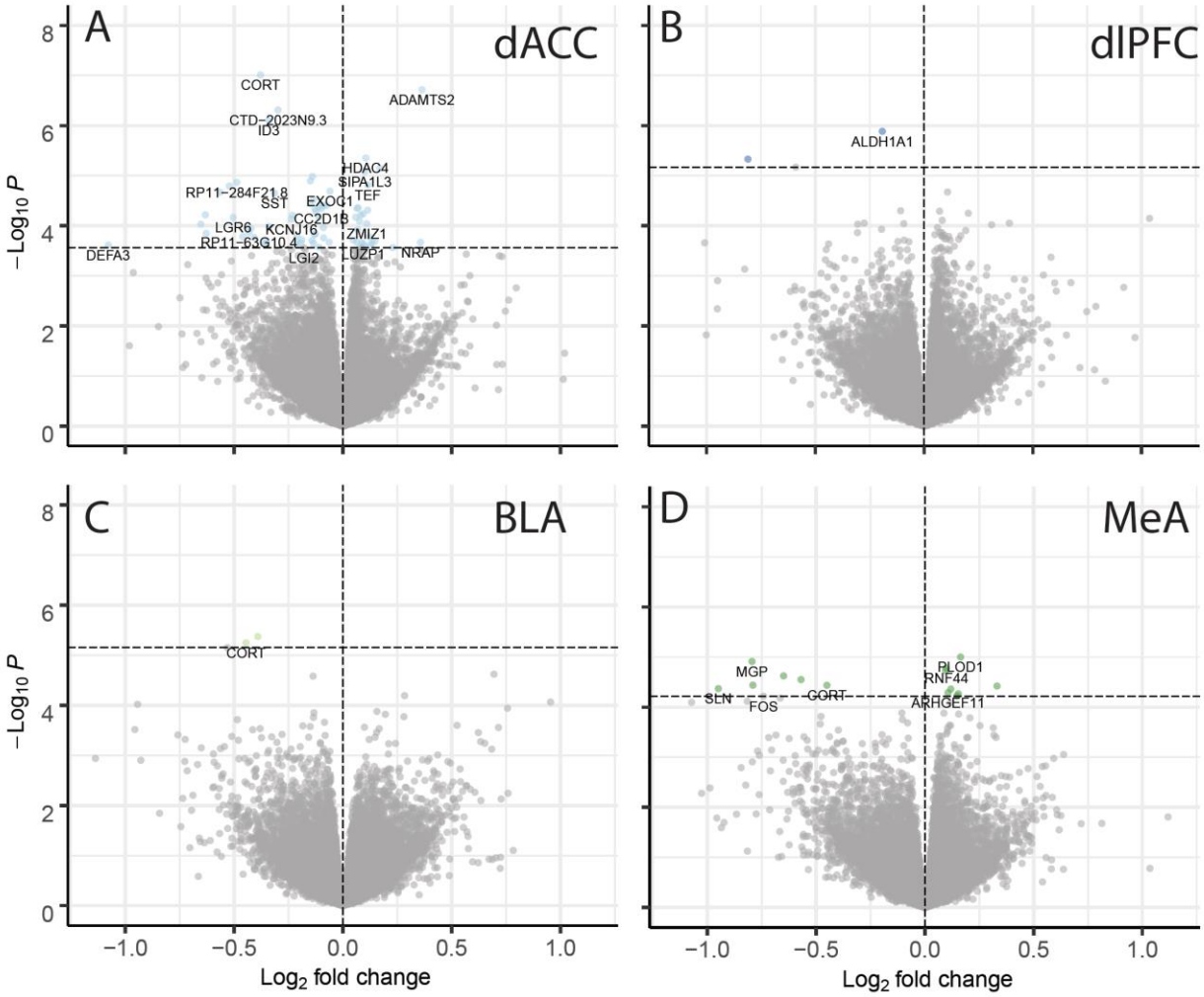

FIGURE S3. Volcano plots by brain subregions, for (A) dACC and (B) dlPFC in the cortex and the (C) BLA and (D) MeA in the amygdala. Horizontal lines represent p-values that control FDR < 0.1.

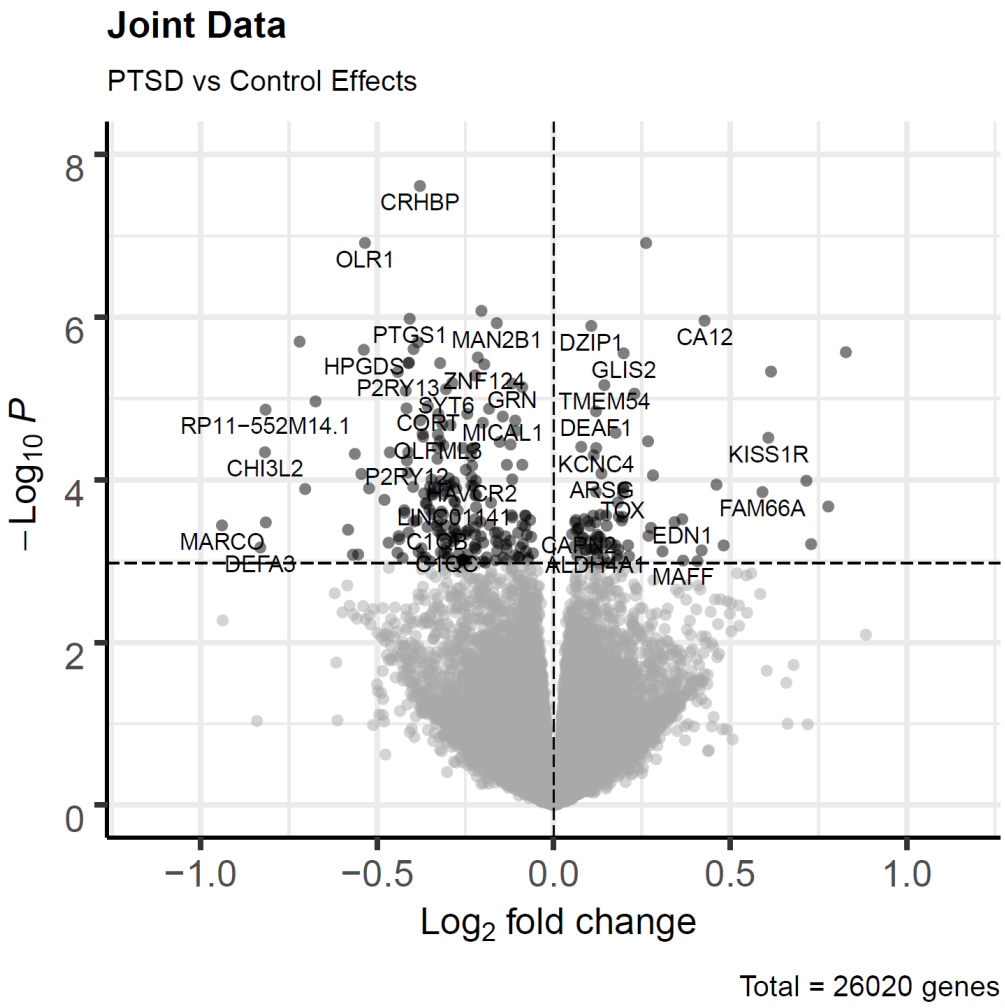

FIGURE S4. volcano plot across all regions.

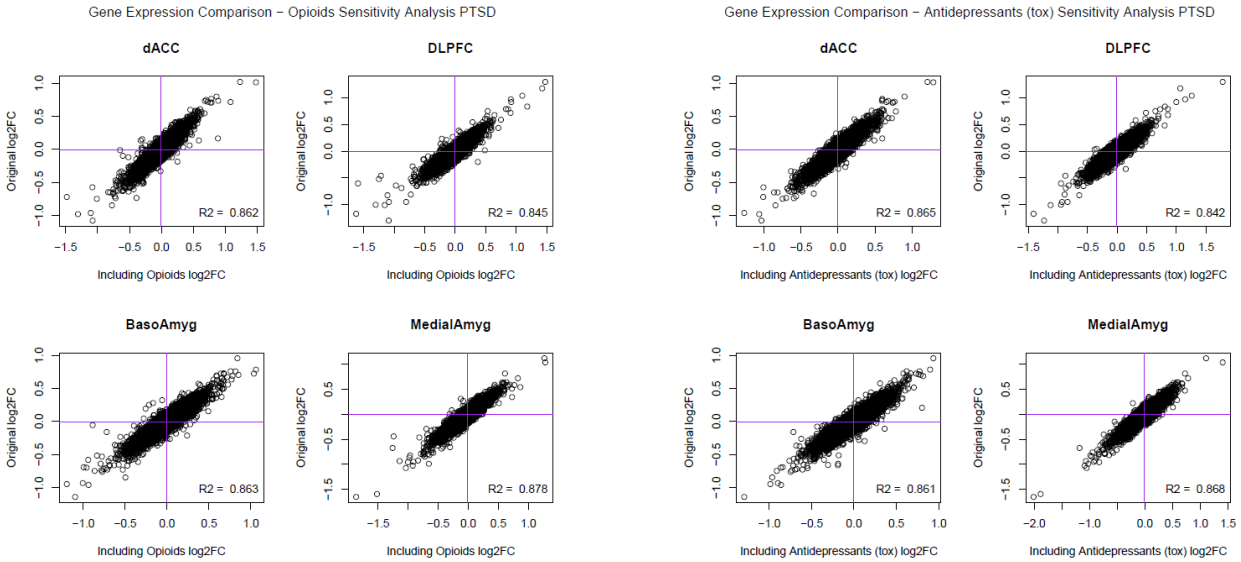

FIGURE S5. Sensitivity analyses for PTSD effects further adjusting for A) opioid and B) antidepressant exposures, in addition to all other considered observed and latent confounders described in the Methods section.

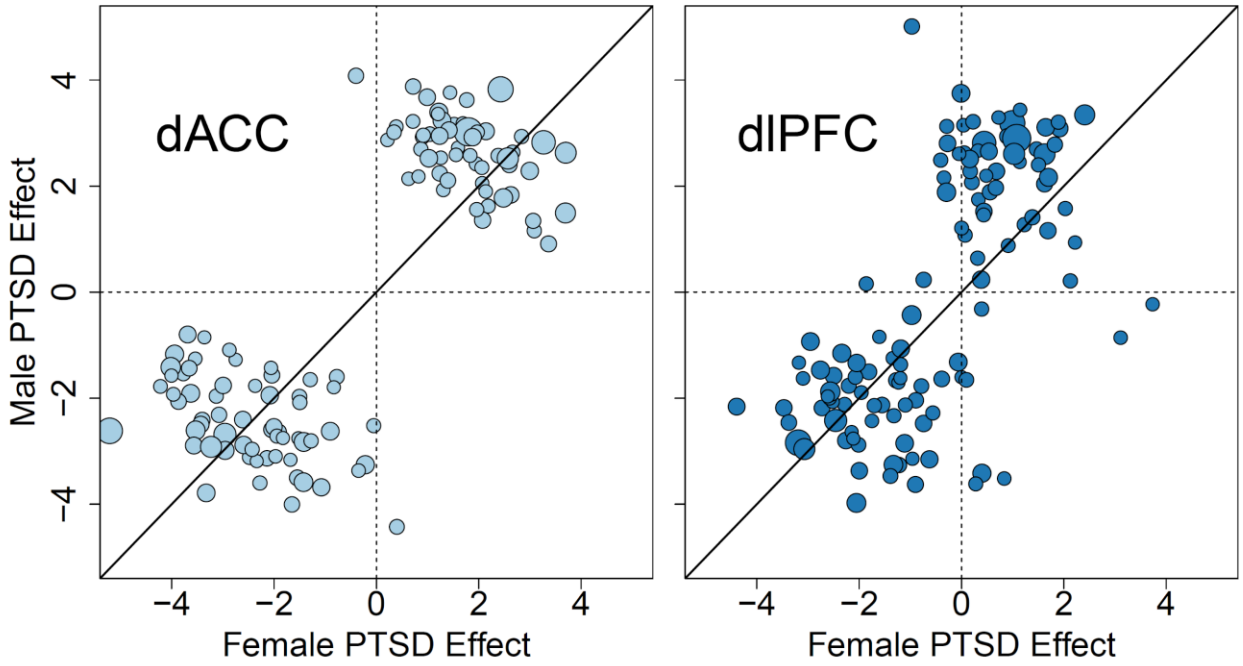

FIGURE S6. Differences in PTSD effects across the two sexes in the two cortical brain regions. Effects shown are T-statistics.

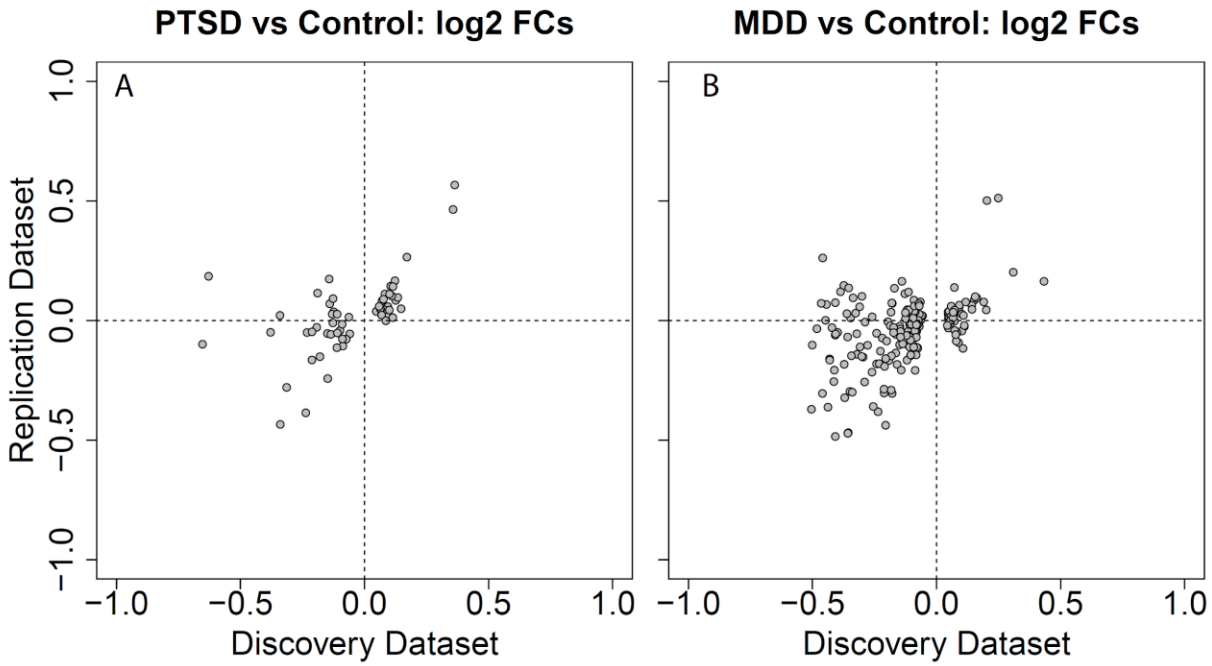

FIGURE S7. Replication of dACC effects with Girgenti et al 2020 (4). (A) PTSD log2 fold changes and (B) MDD log2 fold changes for DEGs identified here at FDR < 0.1.

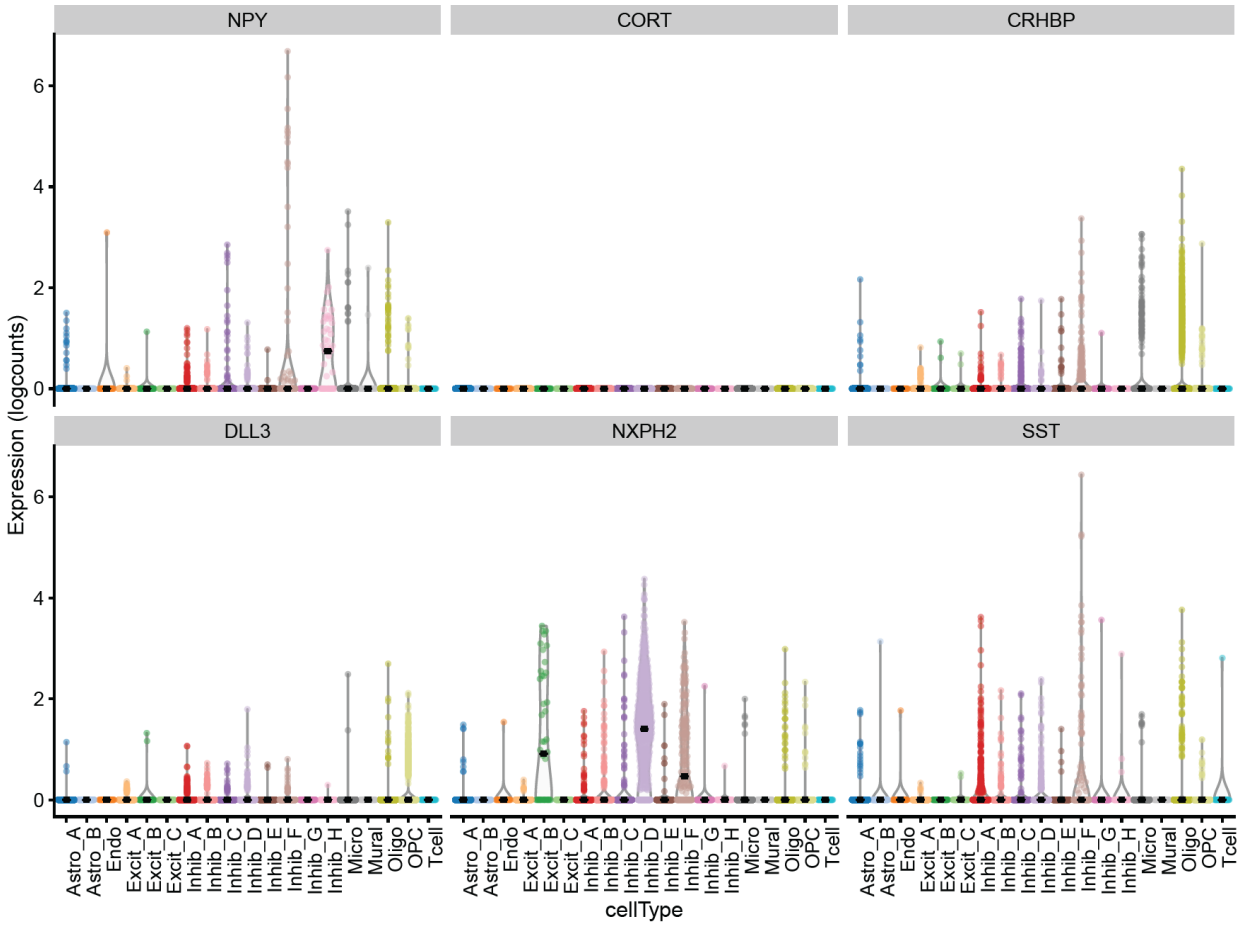

FIGURE S8. Expression of interneuron DEGs in amygdala snRNA-seq data, including *CORT*.

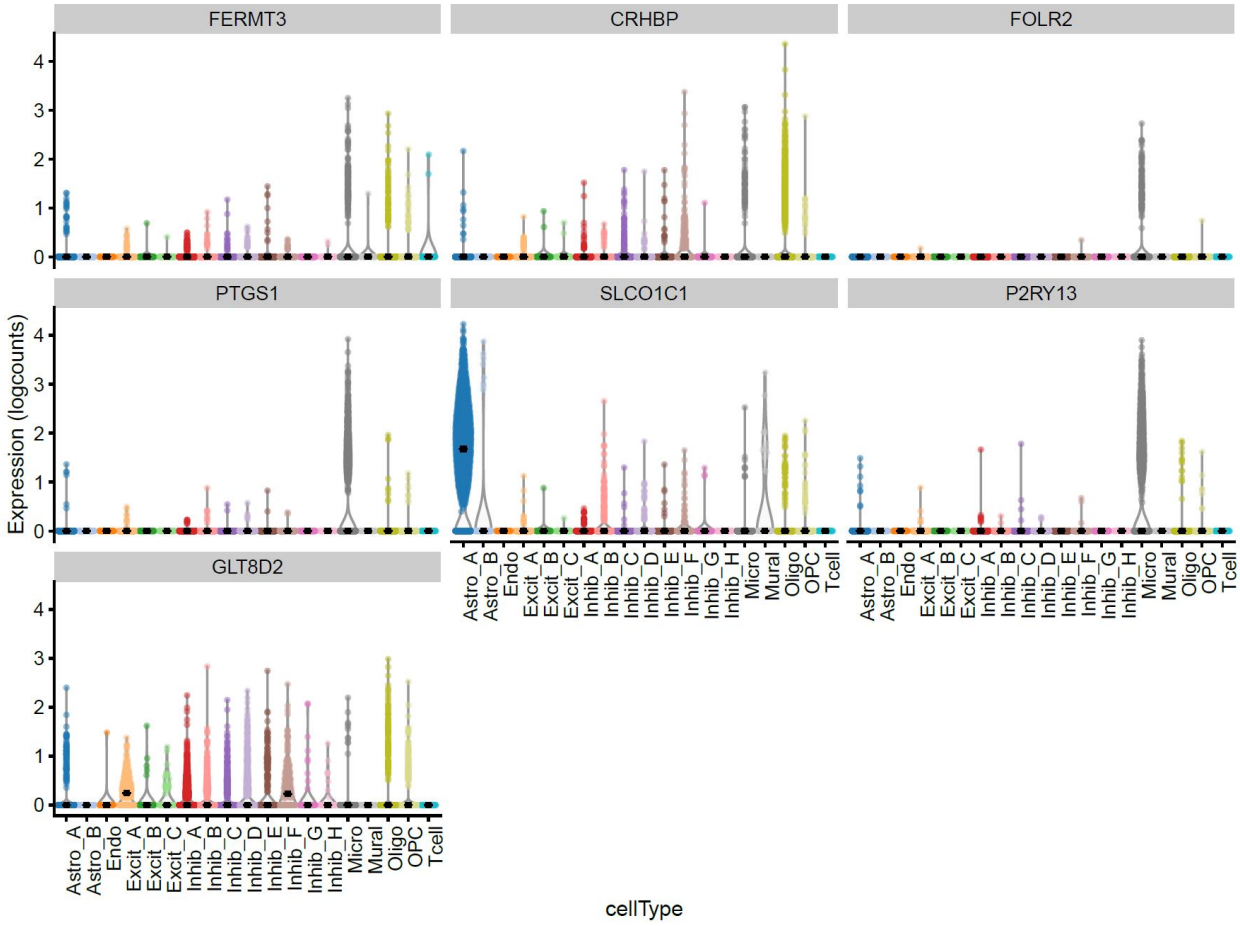

FIGURE S9. Expression of immune-related DEGs in amygdala snRNA-seq data.

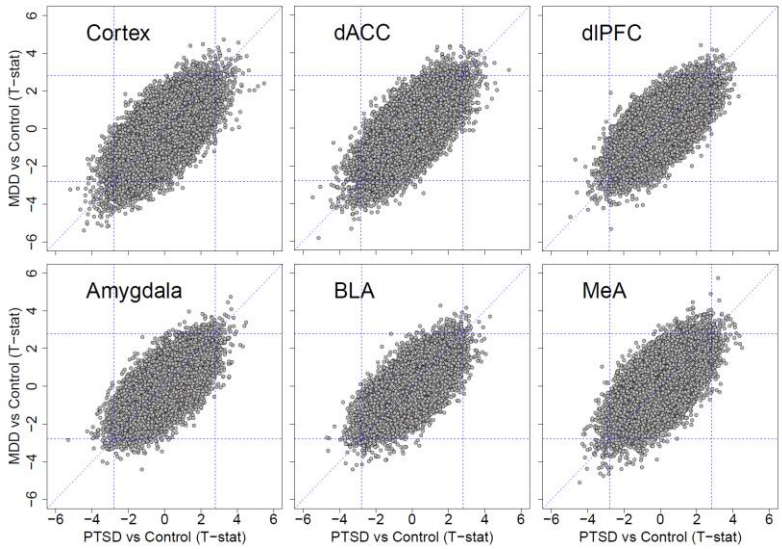

FIGURE S10. High correlation between PTSD and MDD effects across brain regions.

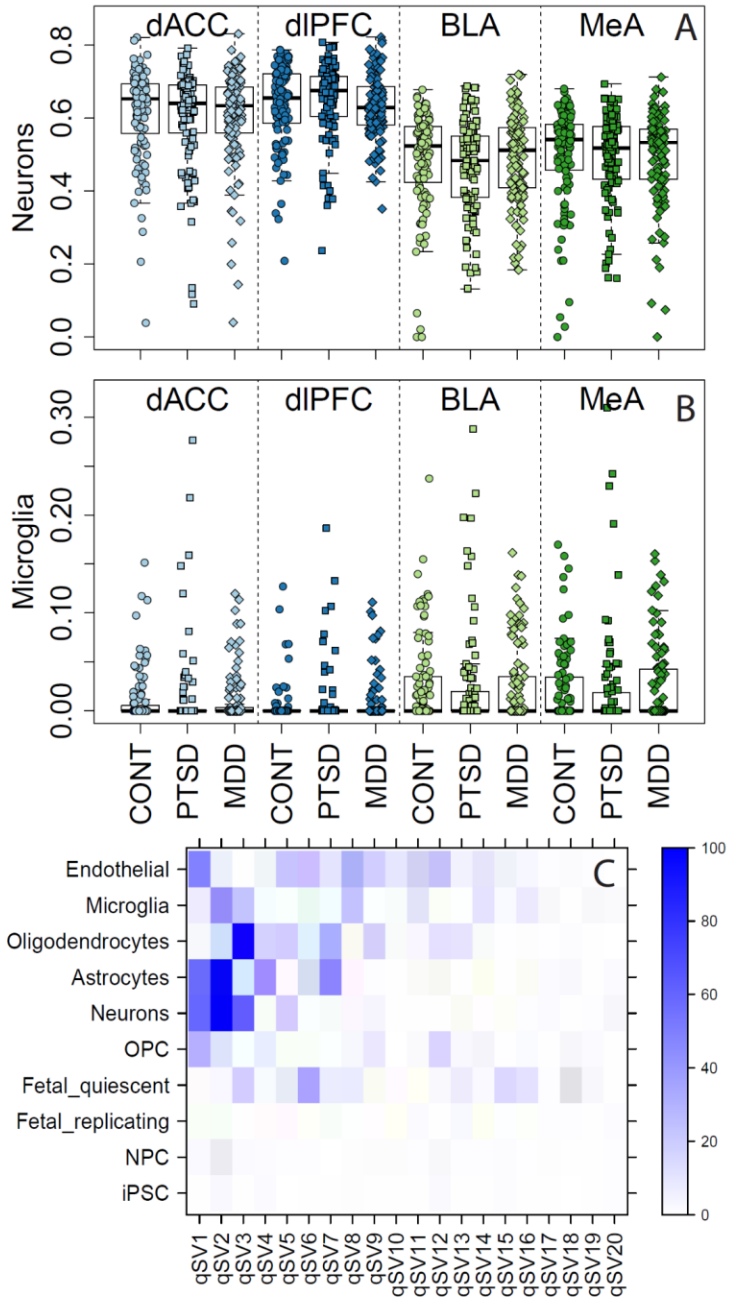

FIGURE S11. Examining the effects of RNA composition on brain region and diagnosis group. RNA fractions of (A) neurons and (B) microglia varied across brain regions but did not differ by diagnosis. (C) Existing modeling strategies incorporating qSVs likely already captured cellular variation. Shown are correlations (as -log10 p-values) between each cell type's RNA fraction and each qSV.

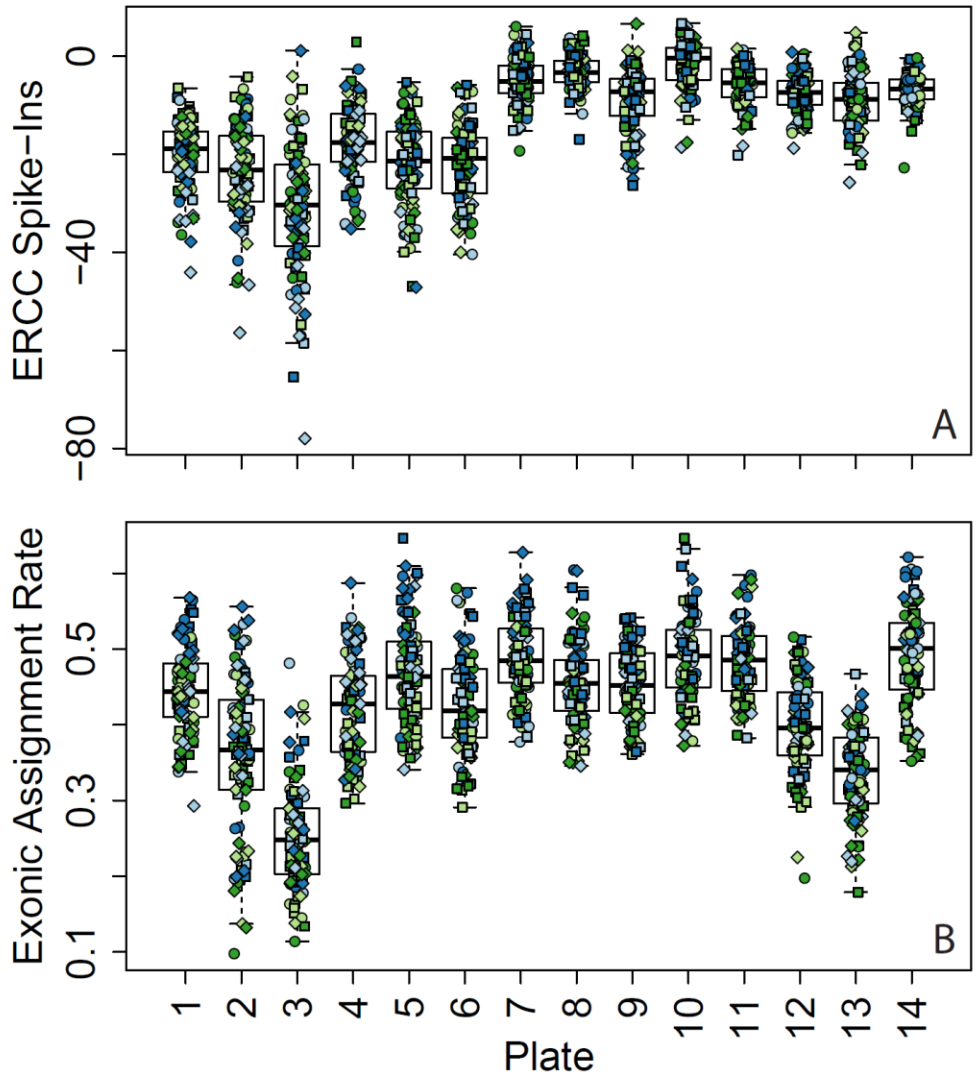

FIGURE S12. Sequencing metrics by processing plate. (A) ERCC Spike-in bias and (B) exonic mapping rates across the 14 processing plates. Colors indicate brain region and shapes indicate diagnostic groups (using same coloring as Figure 1).

References

1. American Psychiatric Association. Diagnostic and Statistical Manual of Mental Disorders. 5th ed. 2013.
2. Von Economo C. Cellular structure of the human cerebral cortex. Karger Medical and Scientific Publishers; 2009.
3. Jaffe AE, Tao R, Norris AL, Kealhofer M, Nellore A, Shin JH, et al. qSVA framework for RNA quality correction in differential expression analysis. Proc Natl Acad Sci USA. 2017 Jul 3;114(27):7130–5.
4. Unable to find information for 8596810.
5. Doyle JP, Dougherty JD, Heiman M, Schmidt EF, Stevens TR, Ma G, et al. Application of a translational profiling approach for the comparative analysis of CNS cell types. Cell. 2008 Nov 14;135(4):749–62.
6. Dougherty JD, Schmidt EF, Nakajima M, Heintz N. Analytical approaches to RNA profiling data for the identification of genes enriched in specific cells. Nucleic Acids Res. 2010 Jul;38(13):4218–30.
7. Xu X, Wells AB, O'Brien DR, Nehorai A, Dougherty JD. Cell type-specific expression analysis to identify putative cellular mechanisms for neurogenetic disorders. J Neurosci. 2014 Jan 22;34(4):1420–31.
8. Skene NG, Bryois J, Bakken TE, Breen G, Crowley JJ, Gaspar HA, et al. Genetic identification of brain cell types underlying schizophrenia. Nat Genet. 2018 Jun;50(6):825–33.
9. Hawrylycz MJ, Lein ES, Guillozet-Bongaarts AL, Shen EH, Ng L, Miller JA, et al. An anatomically comprehensive atlas of the adult human brain transcriptome. Nature. 2012 Sep 20;489(7416):391–9.
10. Mai JK, Paxinos G, Voss T. Atlas Of The Human Brain. 3rd ed. Academic Pr 2007-11-20; 2007.
11. Collado-Torres L, Burke EE, Peterson A, Shin J, Straub RE, Rajpurohit A, et al. Regional Heterogeneity in Gene Expression, Regulation, and Coherence in the Frontal Cortex and Hippocampus across Development and Schizophrenia. Neuron. 2019 Jul 17;103(2):203-216.e8.
12. Kim D, Langmead B, Salzberg SL. HISAT: a fast spliced aligner with low memory requirements. Nat Methods. 2015 Apr;12(4):357–60.
13. Liao Y, Smyth GK, Shi W. featureCounts: an efficient general purpose program for assigning sequence reads to genomic features. Bioinformatics. 2014 Apr 1;30(7):923–30.
14. Feng Y-Y, Ramu A, Cotto KC, Skidmore ZL, Kunisaki J, Conrad DF, et al. RegTools: Integrated analysis of genomic and transcriptomic data for discovery of splicing variants in cancer. BioRxiv. 2018 Oct 5;
15. Kim D, Pertea G, Trapnell C, Pimentel H, Kelley R, Salzberg SL. TopHat2: accurate

alignment of transcriptomes in the presence of insertions, deletions and gene fusions. Genome Biol. 2013 Apr 25;14(4):R36.

16. Jaffe AE, Straub RE, Shin JH, Tao R, Gao Y, Collado-Torres L, et al. Developmental and genetic regulation of the human cortex transcriptome illuminate schizophrenia pathogenesis. Nat Neurosci. 2018 Aug;21(8):1117–25.

17. Patro R, Duggal G, Love MI, Irizarry RA, Kingsford C. Salmon provides fast and bias-aware quantification of transcript expression. Nat Methods. 2017 Apr;14(4):417–9.

18. Bray NL, Pimentel H, Melsted P, Pachter L. Near-optimal probabilistic RNA-seq quantification. Nat Biotechnol. 2016 May;34(5):525–7.

19. Wang L, Wang S, Li W. RSeQC: quality control of RNA-seq experiments. Bioinformatics. 2012 Aug 15;28(16):2184–5.

20. Kent WJ, Zweig AS, Barber G, Hinrichs AS, Karolchik D. BigWig and BigBed: enabling browsing of large distributed datasets. Bioinformatics. 2010 Sep 1;26(17):2204–7.

21. Howie BN, Donnelly P, Marchini J. A flexible and accurate genotype imputation method for the next generation of genome-wide association studies. PLoS Genet. 2009 Jun 19;5(6):e1000529.

22. Delaneau O, Coulonges C, Zagury J-F. Shape-IT: new rapid and accurate algorithm for haplotype inference. BMC Bioinformatics. 2008 Dec 16;9:540.

23. 1000 Genomes Project Consortium, Auton A, Brooks LD, Durbin RM, Garrison EP, Kang HM, et al. A global reference for human genetic variation. Nature. 2015 Oct 1;526(7571):68–74.

24. Purcell S, Neale B, Todd-Brown K, Thomas L, Ferreira MAR, Bender D, et al. PLINK: a tool set for whole-genome association and population-based linkage analyses. Am J Hum Genet. 2007 Sep;81(3):559–75.

25. Collado-Torres L, Nellore A, Frazee AC, Wilks C, Love MI, Langmead B, et al. Flexible expressed region analysis for RNA-seq with derfinder. Nucleic Acids Res. 2017 Jan 25;45(2):e9.

26. Buja A, Eyuboglu N. Remarks on parallel analysis. Multivariate Behav Res. 1992 Oct 1;27(4):509–40.

27. Leek JT, Storey JD. Capturing heterogeneity in gene expression studies by surrogate variable analysis. PLoS Genet. 2007 Sep;3(9):1724–35.

28. Law CW, Chen Y, Shi W, Smyth GK. voom: Precision weights unlock linear model analysis tools for RNA-seq read counts. Genome Biol. 2014 Feb 3;15(2):R29.

29. Yu G, Wang L-G, Han Y, He Q-Y. clusterProfiler: an R package for comparing biological themes among gene clusters. OMICS. 2012 May;16(5):284–7.

30. Ashburner M, Ball CA, Blake JA, Botstein D, Butler H, Cherry JM, et al. Gene Ontology: tool for the unification of biology. Nat Genet. 2000 May;25(1):25–9.

31. The Gene Ontology Consortium. Expansion of the Gene Ontology knowledgebase and

resources. Nucleic Acids Res. 2017 Jan 4;45(D1):D331–8.

32. Kanehisa M, Furumichi M, Tanabe M, Sato Y, Morishima K. KEGG: new perspectives on genomes, pathways, diseases and drugs. Nucleic Acids Res. 2017 Jan 4;45(D1):D353–61.

33. Burke EE, Chenoweth JG, Shin JH, Collado-Torres L, Kim SK, Micali N, et al. Dissecting transcriptomic signatures of neuronal differentiation and maturation using iPSCs. Nat Commun. 2019 Dec 31;

34. Langfelder P, Horvath S. WGCNA: an R package for weighted correlation network analysis. BMC Bioinformatics. 2008 Dec 29;9:559.

35. Collado-Torres L, Jaffe AE. jaffelab: Commonly used functions by the Jaffe lab. GitHub: GitHub; 2018.

36. Tran MN, Maynard KR, Spangler A, Huuki LA, Montgomery KD, Sadashivaiah V, et al. Single-nucleus transcriptome analysis reveals cell-type-specific molecular signatures across reward circuitry in the human brain. Neuron. 2021 Oct 6;109(19):3088-3103.e5.

37. Velmeshev D, Schirmer L, Jung D, Haeussler M, Perez Y, Mayer S, et al. Single-cell genomics identifies cell type-specific molecular changes in autism. Science. 2019 May 17;364(6441):685–9.

38. Mathys H, Davila-Velderrain J, Peng Z, Gao F, Mohammadi S, Young JZ, et al. Single-cell transcriptomic analysis of Alzheimer's disease. Nature. 2019 Jun;570(7761):332–7.

39. Maynard KR, Tippani M, Takahashi Y, Phan BN, Hyde TM, Jaffe AE, et al. dotdotdot: an automated approach to quantify multiplex single molecule fluorescent in situ hybridization (smFISH) images in complex tissues. Nucleic Acids Res. 2020 May 8;

40. Ketchesin KD, Huang NS, Seasholtz AF. Cell Type-Specific Expression of Corticotropin-Releasing Hormone-Binding Protein in GABAergic Interneurons in the Prefrontal Cortex. Front Neuroanat. 2017 Oct 10;11:90.

41. Calakos KC, Blackman D, Schulz AM, Bauer EP. Distribution of type I corticotropin-releasing factor (CRF1) receptors on GABAergic neurons within the basolateral amygdala. Synapse. 2017 Feb 20;71(4).